Crystallization in Zeolite A Studied by Atomic Force Microscopy

Jonathan R. Agger,[†] Noreen Pervaiz,[†] Anthony K. Cheetham,[‡] and Michael W. Anderson*,[†]

Contribution from the Department of Chemistry, UMIST, P.O. Box 88, Manchester M60 1QD, United Kingdom, and Materials Research Laboratory, University of California, Santa Barbara, California 93106

Received May 13, 1998

Abstract: Crystal growth in zeolite A has been studied by atomic force microscopy (AFM), which is a very powerful technique for imaging nanoscale surface features. However, imaging microcrystallites is far from trivial due to the difficulty in controlling their orientation—surfaces inclined to the horizontal yield distorted images in an AFM. In this study the origin and correction of image distortion is discussed and a general method for sample preparation that can be easily adapted to any microcrystalline powder is detailed. Crystal growth in zeolite A, chosen for its industrial importance, is discussed in detail and is shown to occur via a process akin to a terrace−ledge−kink (TLK) layer mechanism.

Introduction

Owing to its excellent ion-exchange capacity and consequent use as a water softening agent in modern-day washing powders, zeolite A boasts the greatest worldwide industrial tonnage of any zeolite. In recent decades, all aspects of the material have been extensively studied. However, akin to every other zeolite, the exact mechanism of its crystallization remains elusive. A detailed understanding of this hydrothermal process would certainly enable more rigorous control over crystal size and habit, which would be of enormous benefit to the detergent industry.

Many techniques have been used to gain an insight into the complex processes occurring between nucleation and completion of crystallization in zeolite A: scanning electron microscopy, transmission electron microscopy, optical microscopy, and powder X-ray diffraction are commonly used to analyze final particle-size distributions and crystallinity;[1−6] elemental analysis may be used to follow the concentrations of silicate, aluminate, and sodium oxide in the liquid phase;[2,6] infrared spectroscopy yields information on structural features;[5] and quasielastic light-scattering spectroscopy of clear gel solutions[7] may be used to follow submicron particles in the parent solutions.[4,5] Various aspects of the synthesis have been studied with these techniques, including crystallization kinetics, gel pH, effect of amorphous seeding, initial bred nuclei, gel aging, and the addition of aged mother liquor.

The advent of atomic force microscopy (AFM), a very powerful technique for imaging nonconducting solid surfaces, now enables the imaging of surface growth features of zeolites. Recently, we briefly reported the first AFM study of a *synthetic* zeolite.[8] AFM images of the FAU and EMT polymorphs of zeolite Y revealed crystal growth terraces: (i) with a constant step height consistent with the known structures and (ii) with orientations, positions, and geometries concurrent with a layer growth mechanism. Imaging of a mineral zeolite AFM was first achieved by Weisenhorn et al. in 1990.[9] Molecular resolution of the cleaved (010) surface of the naturally occurring zeolite clinoptilolite under liquid was attained. Since this early study various groups have looked at cleaved surfaces of the following mineral zeolites: scolecite,[10,11] stilbite,[10−12] faujasite,[10,11] heulandite,[12−15] and mordenite.[16] With the exception of Yamamoto et al.,[15] all of these studies were wholly or partly concerned with imaging at the atomic level to discern structural features or parameters. Both Scandella et al.[13] and Binder et al.[14] observed the existence of cleavage terraces on the surface of heulandite with uniform height equal to half the unit cell length *b*. The most recently published work depicts atomic-scale images of the surface structure of another synthetic zeolite, mordenite.[17]

In this present study atomic force microscopy is employed to image the surface of zeolite A. These images reveal many hitherto unknown details of the mechanism of crystal growth. In general, this detailed study illustrates the power of AFM to investigate crystal growth mechanisms in microcrystalline materials.

[†] UMIST.

[‡] University of California.

(1) Chen, W. H.; Hu, H. C.; Lee, T. Y. *Chem. Eng. Sci.* **1993**, *48*, 3683−3691.

(2) Feoktistiva, N. N.; Vtyurina, L. M. *Russ. Chem. Bull.* **1994**, *43*, 740−745.

(3) Gora, L.; Thompson, R. W. *Zeolites* **1997**, *18*, 132−141.

(4) Gora, L.; Streletzky, K.; Thompson, R. W.; Phillies, G. D. J. *Zeolites* **1997**, *18*, 119−131.

(5) Gora, L.; Streletzky K.; Thompson, R. W.; Phillies, G. D. J. *Zeolites* **1997**, *19*, 98−106.

(6) Antonic, T.; Subotic, B.; Stubicar, N. *Zeolites* **1997**, *18*, 291−300.

(7) Wenqin, P.; Ueda, S.; Koizumi, M. *Proceedings of the 7th International Zeolite Conference*; Elsevier: Amsterdam, 1986; p 177.

(8) Anderson, M. W.; Agger, J. R.; Thornton, J. T.; Forsyth, N. *Angew. Chem., Int. Ed. Engl.* **1996**, *35*, 1210−1213.

(9) Weisenhorn, A. L.; MacDougall, J. E.; Gould, S. A. C.; Cox, S. D.; Wise, W. S.; Massie, J.; Maivald, P.; Elings, V. B.; Stucky, G. D.; Hansma, P. K. *Science* **1990**, *247*, 1330−1333.

(10) MacDougall, J. E.; Cox, S. D.; Stucky, G. D.; Weisenhorn, A. L.; Hansma, P. K.; Wise, W. S. *Zeolites* **1991**, *11*, 429−433.

(11) Occelli, M. L.; Gould, S. A. C.; Stucky, G. D. *Stud. Surf. Sci. Catal.* **1994**, *84*, 485−492.

(12) Komiyama, M.; Yashima, T. *Jpn. J. Appl. Phys.* **1994**, *33*, 3761.

(13) Scandella, L.; Kruse, N.; Prins, R. *Surf. Sci. Lett.* **1993**, *281*, 331−334.

(14) Binder, G.; Scandella, L.; Schumacher, A.; Kruse, N.; Prins, R. *Zeolites* **1996**, *16*, 2−6.

(15) Yamamoto, S.; Sugiyama, S.; Matsuoka, O.; Kohmura, K.; Honda, T.; Banno, Y.; Nozoye, H. *J. Phys. Chem.* **1996**, *100*, 18474−18482.

(16) Yamamoto, S.; Matsuoka, O.; Sugiyama, S.; Honda, T.; Banno, Y.; Nozoye, H. *Chem. Phys. Lett.* **1996**, *260*, 208−214.

(17) Sugiyama, S.; Yamamoto, S.; Matsuoka, O.; Honda, T.; Nozoye, H.; Qiu, S.; Yu, J.; Terasaki, O. *Surf. Sci.* **1997**, *377*, 140−144.

10.1021/ja981665s CCC: $15.00
Published on Web 10/06/1998

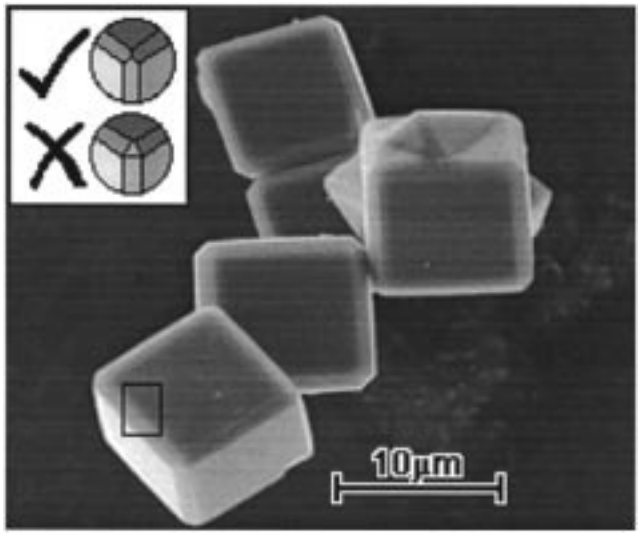

Figure 1. Scanning electron micrograph of zeolite A crystals. The inset highlights the absence of {111} crystal facets. The rectangle shows the approximate orientation of the image shown in Figure 4.

Experimental Section

Sample Preparation. The following procedure was used to prepare relatively large (ca. 10 μm) sized zeolite A crystals: 12.5 g of sodium silicate and 12.5 cm^3 of triethanolamine were dissolved in 87.5 cm^3 of deionized water to form solution A; 10.0 g of sodium aluminate (28.4 wt % Na_2O, 46.7 wt % Al_2O_3) and 12.5 cm^3 of triethanolamine were dissolved in 87.5 cm^3 of deionized water to form solution B. Both solutions were passed through 0.22 μm filters before being combined. The resultant gel was well stirred and then heated at 40 °C for 48 h. The resulting solid was recovered by filtration and washed in ice cold water.

Scanning Electron Microscopy (SEM). Micrographs were obtained a Philips XL30 with field emission gun. Samples were prepared by dusting the zeolite powder onto double-sided carbon tape, mounted on a metal stub. The sample was subsequently sputter coated with a thin carbon film to reduce charging effects.

Atomic Force Microscopy. AFM images (with the exception of Figure 4) were recorded on a Digital Instruments Nanoscope Multimode Microscope operating in TappingMode. The image shown in Figure 4 was recorded a Topometrix Explorer Microscope in high amplitude resonance mode (equivalent to Tappingmode). The method used to prepare the samples for AFM may easily be adapted for fixing any microcrystalline powdered sample. A small quantity of Crystal Bond thermoplastic is placed on a 1 cm diameter metal stub. The stub is placed on a warm hot plate until the thermoplastic becomes malleable and may be flattened with a spatula to provide a smooth surface upon which to apply the sample. It is then left to cool. The powder is sprinkled on the thermoplastic, and microcrystallite distribution and orientation are checked an optical microscope. The stub is placed back on the hot plate until the thermoplastic softens, allowing the crystallites to sink slightly into the surface. Finally the stub is removed and allowed to cool.

By using an optical microscope mounted on the AFM, it is relatively easy to land the tip on crystal faces larger than 10 × 10 μm^2. For smaller crystallites it is usually necessary to land the tip on the thermoplastic close to a crystallite and scan the local area to find the exact location of the crystal face.

A first-order planefit was conducted on the images in the *x* and *y* directions to level the crystal terraces. Dark areas around crystal edges are due to the surface topography possessing a greater slope than the side of the tip. Thus, these areas contain information on the tip shape only and do not contain topographical information.

Results

Figure 1 shows a scanning electron micrograph of the zeolite A used in this study. The crystallites exhibit uniform cubic morphology in the size range 7−15 μm, though some evidence of twinning and intergrowth was found. The square {100} faces can clearly be seen, as can the {110} faces evidenced by the bevelled edges of the cubes. However, the {111} faces have grown out evidenced by the manner in which the bevelled edges meet at the verteces (see inset). This indicates that bulk crystal growth is slower in the ⟨100⟩ and ⟨110⟩ directions than in the ⟨111⟩ directions.

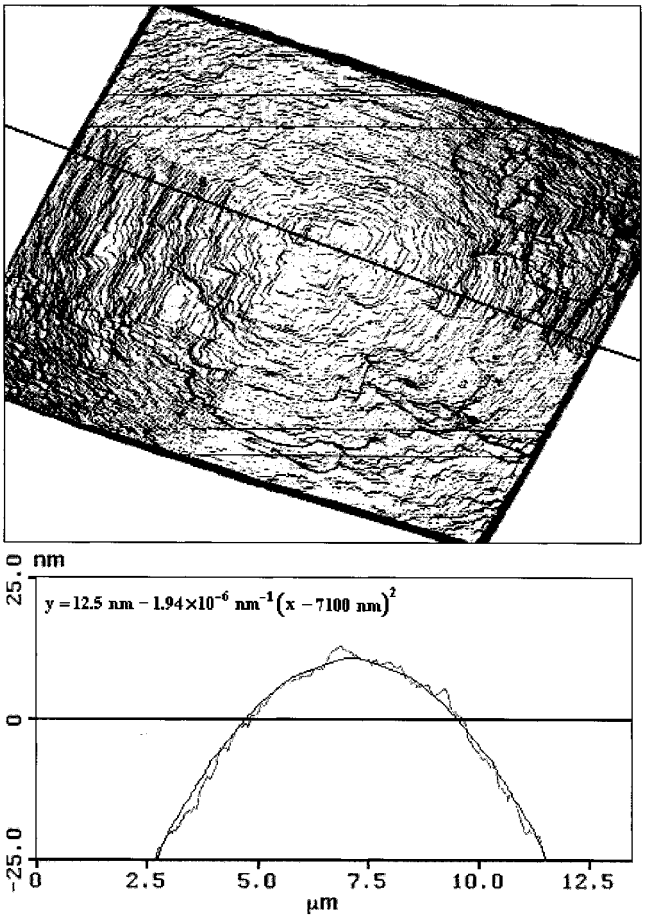

Figure 2. Atomic force micrograph of a 9.0 × 9.0 μm^2 (100) face of a zeolite A crystal with four-quadrant, simulated illumination. The section analysis is taken along the direction of the bold line.

Figure 2 shows an image of a 9.0 × 9.0 μm^2 (100) face. The highest point on the crystal surface is ca. 37.5 nm above the edge of the crystal (as the AFM uses a tube scanner that maps a flat surface onto a spherical surface, we have estimated that this value is correct to within 10%). Beyond the edges are average drops of ca. 5 μm (the crystal is thus embedded in the thermoplastic fixative to a height of ca. 4 μm). If the gray scale table is applied over this full 5 μm height range, the detail of the surface topography is swamped by the relative abyss at the crystal edges. To circumvent this problem, a zero-order flatten (equivalent to a DC offset) has been applied to this image. The horizontal lines, apparent near the top and bottom of the crystal face, are an artifact of this process. To further enhance the detail in the image four-quadrant, simulated illumination has also been used. The image depicts a series of terraces, growing out toward the edge of the crystal, indicative of a layer-growth mechanism. To a first approximation, the layers may be considered tetragonal although many of the verteces are not fully developed. The terrace edges lie parallel to the crystal edges (⟨100⟩ directions). Also shown in Figure 2 is the section analysis of this image taken along the direction of the bold line, showing the 37.5 nm of surface topography across the 9.0 μm span of the crystal.

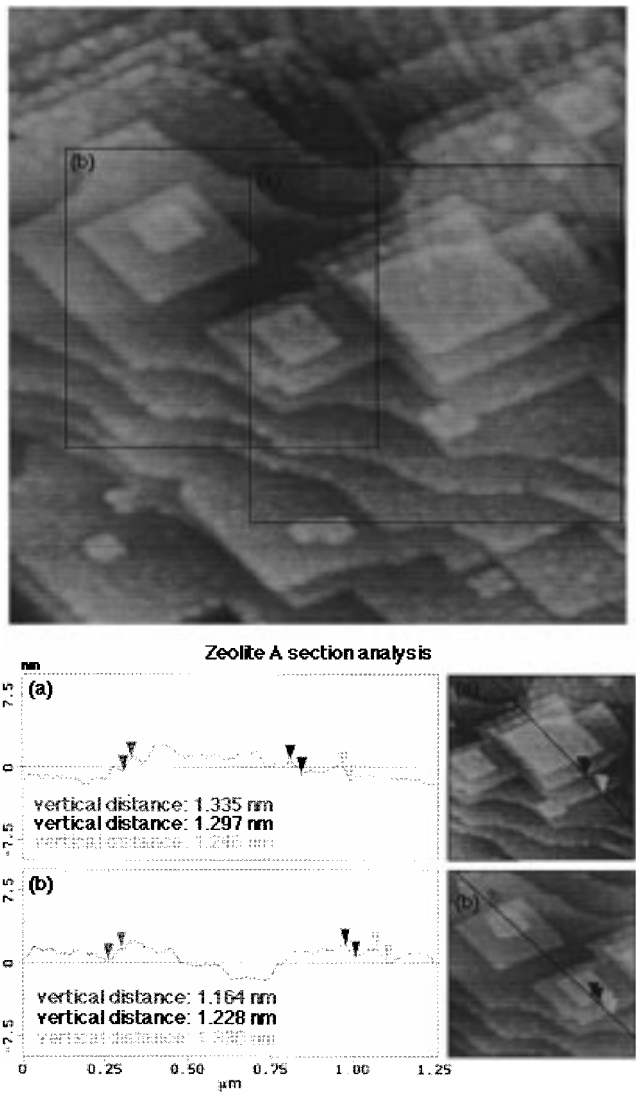

Figure 3. A 1.9 × 1.9 μm^2 atomic force micrograph of the central portion of a (100) face of a zeolite A crystal. Shown in parts a and b are selected areas of this image along with their section analyses.

This image highlights the suitability of atomic force microscopy for extracting information with angstrom vertical resolution.

Figure 3 shows a 1.9 × 1.9 μm^2 scan of the central area of a (100) face of another crystal. At this lateral magnification, the tetragonal crystal terraces can clearly be seen. Parts a and b of Figure 3 show areas of this image (delimited by black boxes) with their corresponding section analyses. These show that the height difference between successive terraces is uniformly equal to 1.20 ± 0.15 nm.

Figure 4 shows an image of a {110} bevelled edge. Of the three faces, the darkest is the (100), the intermediate is the (110), and the lightest is the (010). While square shaped growth terraces can clearly be seen on the (100) face, the (110) face is devoid of any topography other than that caused by surface debris.

Discussion

In Figure 2, it is somewhat surprising to see that the image of the 9.0 × 9.0 μm^2 face is not square in appearance. This is a direct consequence of imaging inclined surfaces. To explain this phenomenon we must understand how the AFM records an image. The following discussion pertains to Figure 5. For a horizontal crystal face (i.e. one perpendicular to the tip) as shown in Figure 5a, the lateral displacement of the tip, as it rasters back and forth across the surface, will be equal to the width of the crystal. In this case there will be no distortion of

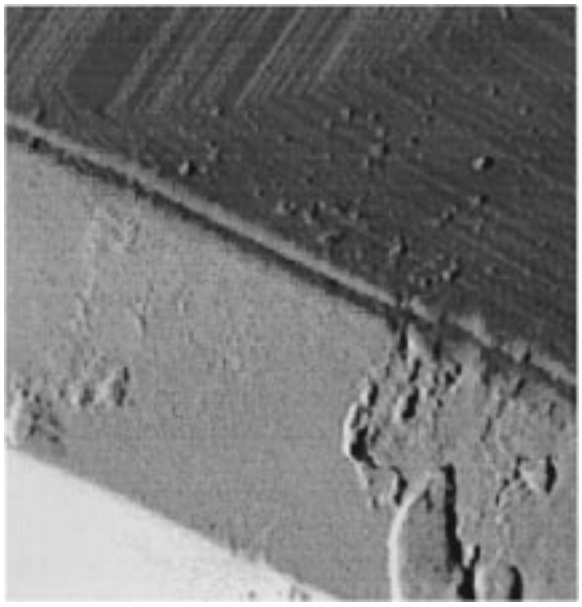

Figure 4. Atomic force micrograph of a bevelled (110) face of a zeolite A crystal. The approximate orientation of this image is given by the rectangle in Figure 1.

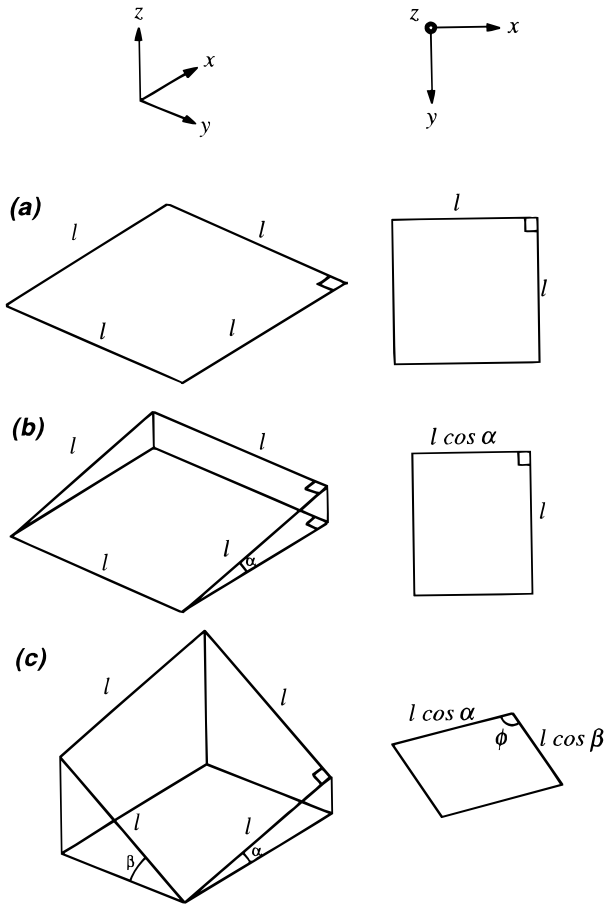

Figure 5. The right-hand diagrams depict the results of an AFM projecting the square shaped feature, with various inclinations shown on the left, onto the horizontal plane. Part a shows the undistorted image of a horizontal feature. Part b shows the slightly distorted image of a feature inclined at an angle α to the horizontal. Part c shows the heavily distorted image of a feature inclined at angles α and β to the horizontal.

the image—the square face will indeed appear to be square. If we now consider the crystal face to be inclined at an angle α to the horizontal, as shown in Figure 5b, then the lateral displacement will now become the width of the crystal multiplied by $\cos \alpha$. Thus the square face will be distorted to a rectangle in the image. The greater the angle of inclination, the more severe the distortion, though the nature of the cosine function dictates that small inclinations result in only very small distortions. To adequately describe the real tilt of a crystal face, the angles of inclination of two adjacent sides of that face from the horizontal are required. Therefore, addition of a second inclination angle, β, is considered in Figure 5c. Now the rectangle becomes a parallelogram (or in the special case where $\alpha = \beta$, a rhombus). By using simple trigonometry the two inclination angles may be determined from the ratio of the edge lengths ($l \cos \alpha / l \cos \beta$) and the angle ϕ. The crystal face in Figure 2 possesses inclination angles of 12.9 and 41.1°. Thus the normal to the surface is tilted at an angle of 44.0° to the vertical movement of the microscope stage. The edge lengths are thus distorted from 9.0 μm to 8.8 μm and 6.8 μm. The use of a tilting stage to orient the crystal under the cantilever tip would remove the need for such data manipulation.

Perhaps of greater significance is the overall form of the section analysis, which is found to be parabolic—the fitted curve being described by the following equation in which x and y, half the crystal terrace edge length and the height above the edge of the crystal, respectively, have been measured in nanometers:

$$y = 12.5 \text{ nm} - (1.94 \times 10^{-6} \text{ nm}^{-1})(x - 7100 \text{ nm})^2 \quad (1)$$

The terms 12.5 nm and −7100 nm serve to position the curve exactly on the scale given by the section analysis, but in its simplest form the equation reduces to:

$$y = (-1.94 \times 10^{-6} \text{ nm}^{-1})(x)^2 \quad (2)$$

Removal of the distortion due to inclination of the crystal face yields:

$$y = (-1.85 \times 10^{-6} \text{ nm}^{-1})(x)^2 \quad (3)$$

The minus sign is simply due to the inverted nature of the parabolic section analysis; however, the constant 1.85×10^{-6} nm^{-1} or 1850 m^{-1} is of greater consequence. The variation of x from zero to half the crystal edge length, $l/2$, necessitates the division of this constant by four to consider the square term as the crystal-terrace area. This yields the value 4.63×10^{-7} nm^{-1} or 463 m^{-1}, which describes the immutable ratio of the rate of surface nucleation, or growth outward from the crystal surface, to the rate of propagation of the area of the crystal surface. Clearly, the greater its value, the more bowed the appearance of the crystal faces. The value presented here is sufficiently small to prevent any visible perception of bowing of the crystal faces by scanning electron microscopy, even with the use of a field emission gun. A typical crystal edge length in an on-screen SEM image is ca. 5 cm, corresponding to a crystal face area of 25 cm^2. Such a face would exhibit a bow of only ca. 0.2 mm.

The explanation for this implied quadratic relationship between the width of a terrace and its height above the crystal edge is founded upon two basic assumptions: (i) The rate of surface nucleation is constant. This implies that if each terrace is uniform in height, as is found to be the case (1.2 nm as indicated in the results section—this will be subsequently discussed), then terrace height above the crystal edge may be used as a measure of time. (ii) Growth occurs via a terrace−ledge−kink (TLK) mechanism.[18] Thus, propagation of the surface terraces occurs via deposition of gel nutrient at constant area kink sites in the terrace ledges. This implies a linear relationship between terrace area and time which further implies a quadratic relationship between terrace width and time. The two assumptions are validated by the excellent fit of the experimental data to this theoretical model. In a previous study, concerned with the growth of zeolite Y crystals—for which the surface terraces are triangular in nature—we were able to show the quadratic dependence of any linear measure of terrace size with terrace height.[8] We now therefore confirm the applicability of a TLK surface-growth mechanism to a second distinct zeolite with completely different crystal morphology.

These AFM results confirm and amplify previous suggestions of layer growth in zeolites. In 1991 Vaughan hinted at the possibility of layer growth in zeolites through an analysis of intergrowth structures.[19] However, the first direct experimental evidence for a layer growth mechanism in zeolite synthesis appeared in two papers published concurrently by Terasaki et al.[20] and by Alfredsson et al.[21] Both papers included high-resolution transmission electron micrographs (HRTEM) of zeolite surface steps. The former showed 14.2 Å high steps on an (001) face of EMT while the latter showed 14.3 Å high steps on a (111) face of FAU. In both cases, each step comprises one faujasite layer. A further concurrent paper was published in 1993 by Burkett et al. on the role of crown ethers in the syntheses of FAU and EMT[22] in which layer-by-layer growth was implied.

In Figure 3, which shows the central area of a crystal face, the growth terraces can clearly be seen. Again, the inclination of the face has resulted in distortion of the image—the two inclination angles of 25.2 and 38.8° being responsible for the parallelogram habit of the terraces. The normal to the surface is tilted at an angle of 49.3° to the vertical movement of the microscope stage. With regard to the uniform terrace-step height of ca. 1.2 nm, inspection of the structure of zeolite A reveals this distance to be equal to half the unit cell dimension of 2.46 nm. The factor of 2 derives from the constraints of superposition of the unit cell (the alternation of silica and alumina primary building units (PBUs) necessitates a doubling of the size of the cell). This implies that each terrace comprises the equivalent of one layer of sodalite cages and one layer of double-four-rings (D4Rs). Such a structure is shown schematically in Figure 6, which depicts four crystal terraces. It is noteworthy that the third terrace (counting from the bottom upward) also contains one of the kink sites mentioned in the previous paragraph, as shown by the arrows. It is not possible from AFM data to ascertain where the bulk structure terminates; however, termination with a layer of sodalite cages as shown in Figure 6a or with a layer of D4Rs as shown in Figure 6b exposes the lowest number of surface atoms and these are therefore two likely possibilities. To address this problem we intend to perform lattice energy minimization calculations on the structure.

Since the visible facets of a crystal are invariably characterized as having the slowest propagation rates, the square nature of the terraces seen in Figure 3 indicates that on the crystal

(18) Burton, W. K.; Cabrera, N.; Frank, F. C. *Philos. Trans. R. Soc. A* **1951**, *243*, 299−358.
(19) Vaughan, D. E. W. *Stud. Surf. Sci. Catal.* **1991**, *65*, 275−286.
(20) Terasaki, O.; Ohsuna, T.; Alfredsson, V.; Bovin, J.-O.; Watanabe D.; Carr, S. W.; Anderson, M. W. *Chem. Mater.* **1993**, *5*, 452−458.
(21) Alfredsson, V.; Ohsuna, T.; Terasaki, O.; Bovin, J.-O. *Angew. Chem., Int. Ed. Engl.* **1993**, *32*, 1210−1213.
(22) Burkett, S. L.; Davis, M. E. *Microporous Mater.* **1993**, *1*, 265−281.

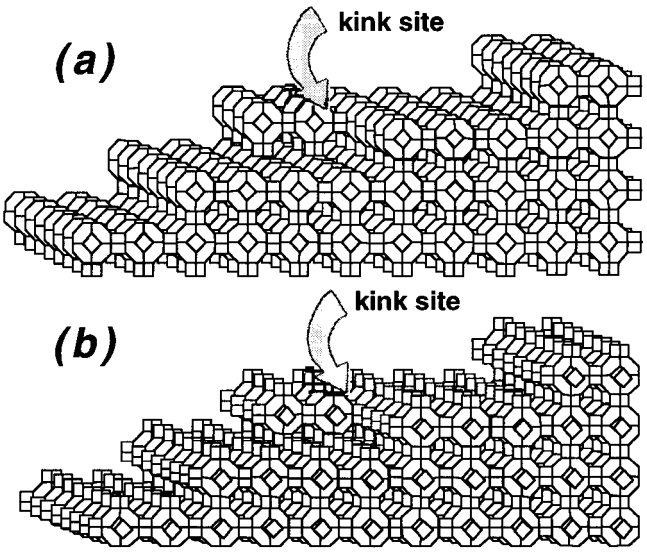

Figure 6. Schematic representation of the growth structure of zeolite A comprising four layers of sodalite cages and D4Rs. Part a shows the surface terminated in sodalite cages while part b shows it terminated in D4Rs. In both cases a kink site may be seen in the third layer counting upward from the bottom. These are pinpointed by arrows.

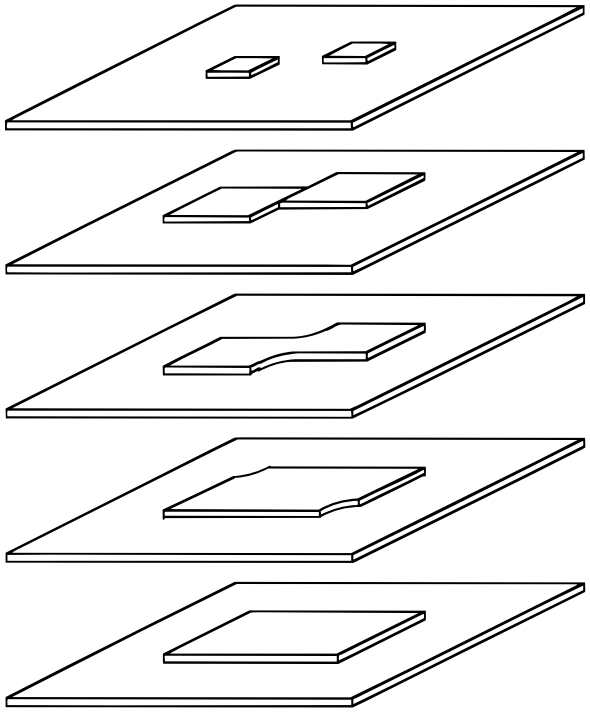

Figure 7. Schematic representation showing how the coalescence of multiple nucleation points may result in crystal terraces with curved verteces.

surface, the ⟨010⟩ and ⟨001⟩ directions propagate most slowly. Apparent in the images, however, are incomplete verteces, evidenced by the curved terrace edges. The possibility that these curved terrace edges might be a dissolution effect may be discounted on the grounds of work by Yamamoto et al.[15] In an AFM study of the dissolution of heulandite in both acidic and alkaline aqueous solutions they found the process to occur via the formation of pits in the exposed layer, and in neither case did they witness step retreat. We therefore believe these curved edges to be a growth effect and to be a direct consequence of the presence of multiple nucleation points. As can be seen in Figure 3, a high density of nucleation points for

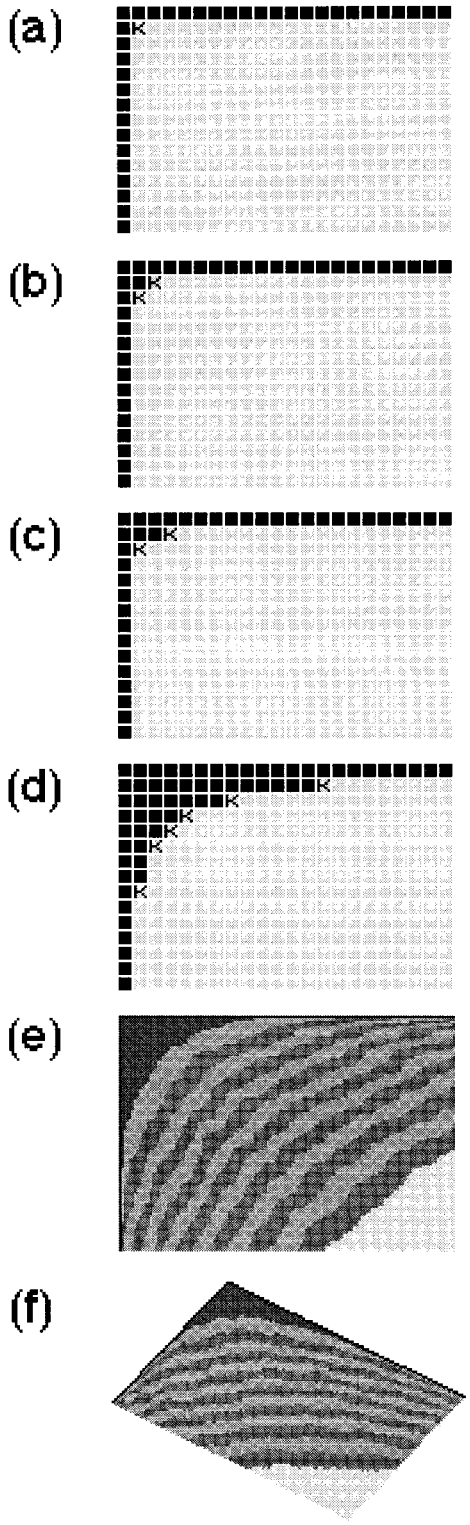

Figure 8. Schematic representation of the Monte Carlo simulation showing the following: (a) creation of the coalescence grid and the first kink site denoted ***K***; (b) deposition of a basic building unit (BBU) at the aforementioned kink site, with subsequent creation of two further kink sites; (c) deposition of a second BBU at one of the two kink sites, chosen at random, with equal probability; (d) a later stage of the simulation showing progression of the growth front, the next BBU will be placed at random at one of the six kink sites, again with equal probability; (e) the final simulation, in which the progressive shape of the growth front has been highlighted by means of periodic color change; (f) a change of the view point may be used to simulate inclination of the crystal face.

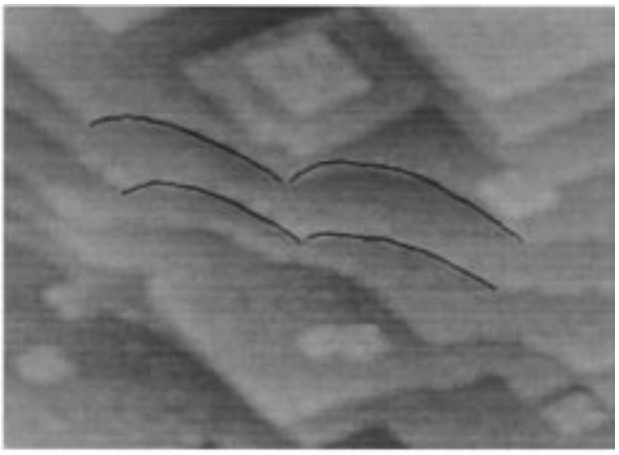

Figure 9. Simulated growth fronts transcribed onto the curved verteces of the terraces shown in Figure 3.

each new terrace on any given {100} surface exists. As these multiple nucleation points grow outward they maintain their square shape until the onset of coalescence, at which point a kink site for growth in all other directions is created. The intermediate stages of coalescence are thus characterized by the curved terrace edges witnessed. A pictorial representation of this process is shown in Figure 7. To further investigate this concept, we have performed Monte Carlo simulation of the evolution of such a coalescence point, by means of a program written in MATHEMATICA from Wolfram Research Inc. A pictorial representation is given in Figure 8.

As can be seen in Figure 7, at the coalescence point, an area is formed that is bounded on two sides by the square terraces. To simulate this, a coalescence grid is created, the size of which is determined by the numbers of basic building units (BBUs) along each edge. We intend BBU to mean one-eighth of the unit cell for zeolite A, i.e., a sodalite cage with three double-four rings, the dimensions of which are $1.2 \times 1.2 \times 1.2$ nm^3 (it should be noted that the BBU used for the calculation is not considered to be the building unit formed in solution). The two coalescing terraces are simulated by filling two adjacent edges of the grid with BBUs, Figure 8a. The rest of the simulation is iterative. In each iteration, the program locates kink sites, Figures 8a−d. Each kink site is assigned a probability for deposition of the next BBU equal to $1/n$, where n is the number of kink sites identified in that iteration. This is equivalent to diffusion-limited deposition of growth units as expected in the final stages of crystal growth when the growth nutrient is depleted. A BBU is then placed, at random, at one of the n kink sites, Figures 8, parts b and c. This completes one iteration. Every ith iteration, the plotting color is changed to highlight the progress of the growth front, Figure 8e. The 3D viewpoint is then chosen to mimic the distortion in the image due to the inclination of the crystal face under consideration, Figure 8f.

The simulation clearly corroborates the hypothesis of curved terrace verteces as evidenced by the progressive form of the growth front witnessed in Figure 8f. Continued evolution of a coalescence point results in a lessening of curvature of the advancing terrace. Figure 9 shows the superposition of four such simulated growth fronts upon the curved terrace verteces evident in Figure 3. In each case the size of the correct coalescence grid to use was carefully calculated from the image, taking into account lateral distortion caused by inclination of the crystal face. Clockwise from the top left, the coalescence grids for the four fits have dimensions of 223×338, 262×372, 243×338, and 194×293 in terms of BBUs, respectively. As can be seen, the fit is excellent in every case.

Conclusions

Notwithstanding the obvious differences in the crystal morphologies of zeolites A and Y, close parallels may be drawn between their crystal growth mechanisms. Both zeolites grow by means of a layer mechanism, in each case the layer thickness being closely related to structure. In the case of zeolite A, each layer comprises the equivalent of a sheet of sodalite cages and D4Rs. Both zeolites also show a linear relationship between terrace height and terrace area, indicative of a terrace−ledge−kink mechanism. The striking crystal growth similarities between these two very different zeolites necessitate the study of further zeolite crystals in this manner.

This study highlights the principal difficulty encountered in trying to image micron-sized crystals, i.e., that of orientation of the crystal face with respect to the tip direction. This is a far from trivial point bearing in mind the vast majority of AFM studies are performed on horizontal surfaces. However, we have also shown how the distortion in the image is brought about and consequently how it may be corrected. Simulation of the curved terrace verteces via Monte Carlo modeling confirms kink site growth.

The power of atomic force microscopy to highlight crystal growth features in zeolites has been demonstrated. The technique itself is capable of an order of magnitude greater resolution than we have employed in this study—ultimately to the level of atomic corrugation. It is our belief that such high-resolution imaging may usefully be employed to study molecular decoration of zeolite surfaces, i.e., templating effects.

Acknowledgment. We should like to thank the EPSRC for the funding of N.P. We are grateful to Mr. S. Bennet and Dr. A. Murray for taking the images shown in Figures 1 and 4, respectively. Thanks are also due to Prof. R. Newman for the use of the Digital Instruments AFM and to the experimental officer Mr. J. Walton for his assistance. Finally we are indebted to Dr. S. J. Weigel for preparing the zeolite A sample.

JA981665S